6-1-2016

Surface permeability of natural and engineered porous building materials

David Grover
University of Vermont

Cabot R. Savidge
University of Vermont

Laura Townsend
University of Vermont

Odanis Rosario
University of Vermont

Liang Bo Hu
The University of Toledo

See next page for additional authors

Recommended Citation

Grover D, Savidge CR, Townsend L, Rosario O, Hu LB, Rizzo DM, Dewoolkar MM. Surface permeability of natural and engineered porous building materials. Construction and Building Materials. 2016 Jun 1;112:1088-100.

Authors
David Grover, Cabot R. Savidge, Laura Townsend, Odanis Rosario, Liang Bo Hu, Donna M. Rizzo, and Mandar M. Dewoolkar

SURFACE PERMEABILITY OF NATURAL AND ENGINEERED POROUS BUILDING MATERIALS

David Grover[1], Cabot R. Savidge[2], Laura Townsend[3], Odanis Rosario[4], Liang-Bo Hu[5], and Donna M. Rizzo[6], and Mandar M. Dewoolkar[7*]

[1]Former Graduate Research Assistant, Civil & Environmental Engineering, The University of Vermont, 33 Colchester Ave., Burlington, VT 05405, USA, davidkgrover@gmail.com
[2]Former Graduate Research Assistant, Civil & Environmental Engineering, The University of Vermont, 33 Colchester Ave., Burlington, VT 05405, USA, csavidge@ner.com
[3]Former Undergraduate Researcher, Civil & Environmental Engineering, The University of Vermont, 33 Colchester Ave., Burlington, VT 05405, USA, Laura.Townsend@aecom.com
[4]Former Undergraduate Researcher, Civil & Environmental Engineering, The University of Vermont, 33 Colchester Ave., Burlington, VT 05405, USA, odanis.rosario@gmail.com
[5]Assistant Professor, Department of Civil Engineering, University of Toledo, 2801 W. Bancroft St, Toledo, OH 43606, USA, Liangbo.Hu@utoledo.edu
[6]Professior, Civil & Environmental Engineering, The University of Vermont, 33 Colchester Ave., Burlington, VT 05405, USA, drizzo@uvm.edu
[7]Associate Professor, Civil & Environmental Engineering, The University of Vermont, 33 Colchester Ave., Burlington, VT 05405, USA, mdewoolk@uvm.edu

***Corresponding Author**:

Mandar M. Dewoolkar, Ph.D., P.E.
Associate Professor
Civil and Environmental Engineering
The University of Vermont
213A Votey Hall, 33 Colchester Ave.
Burlington, VT 05405
Phone: 1-802-656-1942
E-mail: mdewoolk@uvm.edu

Abstract

Characterization of surface gas permeability measurements on a variety of natural and engineered building materials using two relatively new, non-destructive surface permeameters is presented. Surface gas permeability measurements were consistent for both laboratory and field applications and correlated well with bulk gas permeability measurements. This research indicates that surface permeability measurements could provide reliable estimates of bulk gas permeability; and due to the non-destructive nature and relative sampling ease of both surface gas permeability tools, it is possible to quantify the range of the spatial autocorrelation, heterogeneity, and anisotropy in porous building materials and their degree of degradation from weathering.

Key words: building materials; porous media; surface permeability; non-destructive techniques; weathering; autocorrelation; geostatistics

1. INTRODUCTION

Fluid transport through porous materials is an area of study relevant to many scientific and engineering disciplines such as hydrogeology, geoenvironmental engineering, petroleum engineering, chemical engineering, physics, biology and medicine (e.g. Dandekar, 2006; Dullien, 1992; Gladden et al., 2003; Jang et al., 2003; Steele and Heinzel, 2001). Understanding of permeability and its spatial variability is critical for reliable characterization and prediction of fluid transport. As a result, there is increasing interest in quantifying the aqueous and gaseous permeabilities of natural and engineered porous materials for many practical applications including the durability of porous building materials.

Surface permeability measurements of porous building materials are useful in many scenarios. For example, moisture and air movement throughout a building is dependent on the pore structures, porosities and permeabilities of the building materials used in the structure. If the material bulk permeability of an existing structure is needed, coring the material would be required to determine its bulk permeability in a laboratory setting. In such instances, nondestructive surface permeability measurements, already correlated to bulk permeability measurements, would be more convenient. Another example is the exposure to contaminating agents such as acid rain, toxic spills, and possible chemical and biological agent release, to name a few. After being exposed to such contaminating agents, the demolition or removal of structures may not be viable options, especially for those of historic and cultural significance and emergency facilities. In situations where a building material/structure cannot be removed or destroyed, it is highly likely that only the surface of the materials will be available for non-destructive rapid response measurements and characterization. Therefore, understanding how measured surface permeability correlates to bulk permeability, fluid transport, and the durability of building materials is instrumental to the development of effective decontamination strategies. This research evaluated the surface and bulk permeabilities of typical porous building materials, including natural stones (e.g., sandstones and limestones) and engineered materials (e.g. bricks and concrete).

Non-destructive and cost-efficient mini or probe permeametry has become an important tool, which can quickly provide data for both *ex situ* laboratory and *in situ* field permeability measurements (Chandler et al., 1989; Davis et al., 1994; Dreyer et al., 1990; Dutton and Willis, 1998; Eijpe and Weber, 1971; Fossen et al., 2011; Goggin, 1988; Goggin et al., 1993; Hornung and Aigner, 2002; Huysmansa et al., 2008; Iversen et al., 2003; Rogiers et al., 2011; Sharp Jr. et al., 1994). Valek et al. (2000) developed a surface permeability device to examine the difference in permeability of weathered versus cleaned historic sandstone masonry. Filomena et al. (2013) studied sandstone using two permeameter cells suitable for measuring bulk gas permeability in the laboratory and using two mini permeameters designed for measuring surface gas permeability in the field, and found the two to be strongly correlated. Studies that evaluate correlations between surface and bulk permeabilities across a wide range of materials are not available in the literature. Similarly, literature is lacking that correlates data collected using laboratory surface permeameters and those available for field measurements across a wide range of materials.

Most building materials are porous to some degree and have inherent heterogeneities and anisotropy. For example, in natural materials such as sandstone, stratification often results from the depositional processes that occur during formation producing strong directional anisotropy. Whereas, concretes, the most frequently used engineered building materials (Lomborg, 2000), are typically made of similar constituents; however, the variations in mix proportions and curing times result in more heterogeneous pore structures. Many building materials are regularly exposed to weathering and other degradation processes that are initiated along the surface; and the permeating properties have been recognized as critical for their durability (e.g. Figg, 1972; Zaharieva et al., 2003).

In this paper, we investigate surface gas permeability for a broad range of building materials using an AutoScan II surface gas permeameter, which is suitable for laboratory surface permeability measurements at the sub-millimeter scale. Surface gas permeability was measured over a uniform grid on about 20 different building materials. A majority of these datasets were then compared to those collected with a different permeameter more suitable for field applications, TinyPerm II. These two permeameters are unique in that they are non-destructive and capable of measuring a wide range of surface gas permeabilities. Subsequently, we examined the correlation between surface permeability and bulk gas permeability. To assess the effectiveness of these techniques in characterizing the surface permeability measurements, sample data were analyzed geostatistically to extract the spatial autocorrelation, anisotropy and heterogeneous features inherent to many building materials. Furthermore, surface permeabilities for a subset of the materials studied were measured before and after weathering (simulated freeze-thaw in laboratory), and their applicability for assessing the extent of weathering and degradation was evaluated.

In summary, the specific study objectives were to generate a data set of surface and bulk gas permeability measurements on a variety of natural and engineered porous building materials, and assess whether (1) the surface gas permeability measurements of the two permeameters are comparable, (2) surface gas permeability can reliably estimate bulk gas permeability, and (3) the two devices can be used to characterize the building material structure (e.g. spatial autocorrelation, heterogeneity, and anisotropy) and the degree of degradation from weathering (e.g., freeze-thaw).

2. STUDY MATERIALS

This study evaluated both natural (i.e., granite, sandstones, and limestones) and engineered (i.e., concretes, cement, asphalt, and bricks) porous building materials. The majority of the concretes and cementitious mixtures were hand mixed until the ingredients appeared uniformly mixed, subsequently poured into cylindrical molds (70-78 mm in diameter) or small slabs, and moist cured for a minimum of 28 days and in many cases much longer. All concrete surfaces were 'finished' by hand screeding (removing defects and creating a smooth, finished surface), as is typically done in practice. Cylindrical specimens of natural stone were cored from larger pieces. Cylindrical brick, paver, and in some cases, concrete specimens, were cored from commercially available slabs of these materials. The cylindrical specimens were generally either 70 mm or 78 mm in diameter with heights ranging from 40 to 100 mm.

Initial results revealed that both natural weathering and the concrete screeding process affected the surface permeability. Therefore, several centimeters (between 1 and 4 cm) of material were removed from the top and bottom screeded or weathered portions of specimens to retrieve the interior material as the test specimen and create specimens of equal height. A water saw (i.e., table saw fitted with a constant stream of water) was used to help avoid overheating the specimen during cutting. Interior specimens extracted from cores are explicitly identified in the text.

2.1 Natural Materials

The *natural* materials examined in this study include: (1) Ohio Sandstone, (2) Arkose Sandstone, (3) Portland Brownstone, (4) Indiana Limestone of differing colors, (5) Indiana Limestone, (6) Bluestone Sandstone from a local landscaping company, and (7) Granite of unknown origin. Specimens of materials 1 through 4 were acquired from Granite Importers, Inc., and specimens of materials 5 and 6 were acquired from Indiana Limestone Company and a local landscaping company, respectively. In some cases, materials of the same type but from different sources were tested; they are denoted as Specimen 1, Specimen 2, etc. In addition, surface permeability measurements on a slab specimen of (8) Berea Sandstone are also reported here. These raw Berea Sandstone data were collected by New England Research (2013).

2.2 Engineered Materials

The *engineered* materials examined in this study include: (1) Quickrete Ready Mix Concrete, (2) 3,000 psi Concrete, (3) 5,000 psi Concrete, (4) Sakrete High Strength Concrete, (5) Portland Cement (with no added aggregate), (6) premade D04 Concrete, , (7) Red Clay Brick, (8) Red Colored Concrete Paver, (9) Tan Colored Concrete Paver, (10) Concrete Paver, (11) Asphalt recovered from a road excavation, and (12) Concrete of Unknown Origin. Specimens of materials 1 through 5 were prepared in laboratory, specimens of D04 concrete were supplied by the Idaho National Laboratory, specimens of Red Clay Brick were obtained from a brick yard in Vermont, USA, and specimens of materials 8 through 10 were purchased from a hardware store.

The specific compositions of some materials are unknown, although they were selected because they represent commonly used porous building materials. When materials of the same nominal type or composition, but from different batches or sources, were tested, they are denoted as Specimen 1, Specimen 2, etc. Concretes of specified compressive strengths were prepared using recommended recipes, but the strengths were not confirmed through compression testing.

3. METHODS

Surface gas permeability was measured using two relatively new devices, AutoScan II and TinyPerm II. Relevant ASTM standards do not yet exist for these devices. The testing procedures for the two permeameters and for bulk gas permeability measurements are described below. In addition, a subset of the specimens was subjected to 30 water-saturated, freeze-thaw cycles to evaluate the effects of weathering on surface permeability.

3.1 Surface gas permeability using AutoScan II

Fine-scale gas permeability was measured on specimen surfaces in a laboratory setting using the automated surface gas permeameter apparatus AutoScan II (Figure 1) developed by New England Research, Inc., White River Junction, VT, USA (New England Research, 2014). The entire process is computer-controlled via a connected work station; the user defines the measurement locations along a high-precision, 2-D grid as well as the target pressure and flow rates. Measurement data are stored on the work station, and can be processed and plotted with little user interaction. The device is capable of measuring permeability ranging from 0.1 milliDarcy (mD) (9.87×10^{-17} m^2) to 3 Darcy (D) (2.96×10^{-12} m^2) (New England Research, Inc., 2008). Multiple specimens can be tested in a single run and a different measurement grid can be specified for different specimens. The measurement spacing can be as small as 0.5 mm. The testing presented here employed grid spacings ranging between 1 mm and 5 mm. The specific interval for a specimen depended upon the size of the measurement surface area. The permeability probe (Figure 1b) has a tip seal made of soft rubber that is pressed against the specimen at the specified sampling location to prevent leakage between the probe and the specimen surface as pressurized gas flows down through the specimen to the atmosphere in a roughly hemispherical path as depicted in Figure 1c. Nitrogen gas was used in this work per the manufacturer's recommendation. Once steady-state flow through the specimen is achieved, Darcy's law is employed to determine the surface gas permeability using the following equation (neglecting gas slippage and high velocity flow effects):

$$K_{apparent} = \frac{2Q\mu P_{atm}}{aG_o\left(P^2 - P_{atm}^2\right)}, \quad (1)$$

where $K_{apparent}$ is the apparent permeability (L^2), Q is the flow rate of gas at P_{atm} (L^3/T), μ is the gas viscosity (M/LT), P is the injection pressure of the gas (M/LT^2), P_{atm} is the atmospheric pressure (M/LT^2), a is the internal tip-seal radius (L), and G_o is a geometrical factor (dimensionless).

For this work, the apparent permeability was determined using the manufacturer's default settings for gas viscosity (1.78×10^{-5} Pa·s), internal tip-seal radius (0.005 m), and a geometrical factor of 0.0059. AutoScan II varies the gas injection pressure (P) and the flow rate (Q) for each reading until steady-state conditions are achieved before calculating the $K_{apparent}$. The initial P and Q can be adjusted to achieve steady-state conditions more quickly and the maximum time limit for a sample reading can be specified such that the device will not record a measurement unless steady-state conditions have been reached in the allotted time. In cases where permeability varied greatly across a single specimen and measurements could not be obtained in the time allotted, the specimens were rerun with different initial P and Q values.

The measured apparent permeability is then corrected (K_k) for gas slippage effects at low gas injection pressures:

$$K_k = \frac{K_{apparent}}{1 + \left(\frac{B}{P_{mean}}\right)}, \quad (2)$$

where B is the Klinkenberg slip factor and P_{mean} is the mean pressure measurement $P_{mean} = (P+P_{atm})/2$ (Klinkenberg, 1941).

The permeability computed using equation (2) is further corrected (K_o) for high velocity flow effects (turbulence and inertial) using a Forchheimer factor (F_h) (Goggin et al., 1988):

$$\frac{1.0}{K_o} = \frac{1.0}{K_k} - F_h \cdot Q \ , \qquad (3)$$

AutoScan II determines the Klinkenberg and Forchheimer factors at each sample location.

3.2 Surface gas permeability using TinyPerm II

The surface gas permeability was also measured using TinyPerm II (New England Research, 2015) developed by New England Research, Inc. This is a handheld (~1.2 kg, 38cm × 12.5cm × 5cm), portable device (Figure 2a) that measures surface permeability data in the field (Figure 2b) as well as in a laboratory setting. This device has been used by other researchers, e.g. Rogiers et al. (2013) on soils and Filomena et al. (2013) on sandstone. The rubber nozzle at the end of the device is pressed against the specimen to form an airtight seal. The operator then pushes the syringe toward the specimen, which creates a vacuum by removing air from the specimen. By monitoring the syringe volume and the vacuum pulse at the specimen surface, the TinyPerm II calculates a characteristic value (T), which is related to the gas permeability (K in mD) per the following equation (New England Research, Inc., 2008):

$$\mathrm{K} = 10^{\left(\frac{12.8737-T}{0.8206}\right)}. \qquad (4)$$

Typical T values range between 12.5 and 9.5 yielding permeability measurements between 2 mD (1.97 x 10^{-15} m^2) and 10 D (9.87 x 10^{-12} m^2), respectively (New England Research, Inc., 2008). A permeability reading of 10 mD (9.85 x 10^{-15} m^2), which is the manufacturer's suggested lower limit of the measurement capability, takes about five minutes.

Materials with greater permeabilities typically require shorter measurement times. However, some of the materials studied had surface permeabilities below 10 mD, which required 30 minutes or longer to achieve a steady-state flow. For these specimens, TinyPerm II was mechanically supported to avoid operator fatigue and maintain the conditions required for the correct operation of the device.

Of the 17 interior (note that interior refers to the samples with the top and bottom surfaces removed to sample interior surfaces) specimens tested with AutoScan II, 16 were re-sampled using TinyPerm II, which is well suited for field use. In contrast to the 1,296 points measured with AutoScan II on a 35 × 35 grid with 1 mm grid spacing, TinyPerm II measurements were typically taken at 23 locations on the same specimen surface within the 35 mm × 35 mm area with the exception of Granite and Bluestone which had exceptionally low permeability and thus needed only 12 readings. Statistical analysis was performed on both the raw (rather than $\log_{10}$-transformed) measurements and the geometric means (i.e., arithmetic means on the log scale) of AutoScan II and TinyPerm II measurements.

3.3 Bulk gas permeability

The bulk gas permeability was measured in accordance with ASTM D4525-90: Standard Test Method for Permeability of Rocks by Flowing Air (ASTM International, 2002). The Wykeham Farrance permeability cell was used with two identical pressure transducers to measure the pressure drop across the specimen. A high confining pressure (~275 kPa) was applied to the cell to ensure that the air would pass through, and not between, the specimen and the latex membrane encasing it. A regulated supply of compressed air was applied to the specimen, while the exiting airflow was measured with a calibrated bubble-flow meter. This test was repeated five times on each specimen, with the average of the five measurements reported as the measured bulk gas permeability for that specimen. The gas permeability was calculated as:

$$K = \frac{2Q_e P_e \mu L}{\left(P_i^2 - P_e^2\right)A}, \tag{5}$$

where, K is the coefficient of permeability (L^2), Q_e is the exit flow rate of air (L^3/T), P_e is the exit air pressure (M/LT^2), μ is the viscosity of air at temperature of test (M/LT), L is the length of specimen, P_i is the entrance pressure of air (M/LT^2), and A is the cross-sectional area of specimen (L^2).

3.4 Weathering Effects

Five specimens were cored from nine select materials (Ready Mix, 3,000 psi, 4,000 psi, 5,000 psi, and High Strength Concretes, Portland Cement, Red Brick, Indiana Limestone, and Arkose Sandstone) for a total of 45 specimens. All specimens were approximately 75 mm in diameter and 65-100 mm in height and each was subjected to accelerated weathering of 30 simulated freeze-thaw cycles (-24°C to 20°C) while submerged in water within a mechanical refrigeration chamber. The specimens were placed at random locations within the chamber and relocated between cycles to reduce any placement effects within the freeze-thaw chamber. The surface gas permeability of each specimen was measured along a uniform 3 mm grid spacing using AutoScan II before and after the simulated weathering. These results allow an evaluation of the potential for using surface gas permeability technique to quantitatively characterize the effects of weathering.

3.5 Geospatial Statistical Analysis

Surface gas permeability data, especially the large datasets generated by AutoScan II, can be used to assess the heterogeneity and anisotropy of porous materials. In this study, we determine the spatial auto-correlation along the surface of each specimen, using a geospatial semi-variogram analysis developed and coded in MATLAB (Release 2010a, The Mathworks, Natick, Massachusetts, USA). Semi-variance, $\gamma(h)$, in the geostatistical literature, describes spatial patterns between measured observations as a function of the separation distance (i.e. two points closer to each other in space should be more similar). An example of a semi-variogram (for the specimen of Berea Sandstone) can be found in Figure 11, which will be discussed later in greater detail. These patterns are usually described in terms of dissimilarity rather than similarity or correlation. Thus, the spatial dissimilarity between observations separated by a distance h may be defined as:

$$\gamma(h) = \frac{1}{2N(h)} \sum_{i=1}^{N(h)} [u(a)_i - u(a+h)_i]^2$$

where $N(h)$ is the number of data pairs separated by the distance, h, and $u(a)$ and $u(a+h)$ are the parameter values (i.e., surface permeability) at locations (a) and some distance ($a+h$) away (Issaks and Srivastava, 1989; Journel and Huijbregts, 1978).

A semi-variogram plots the variance between surface permeability measurements against the distance between paired measured values. These paired data are assembled into bins defined by ranges of separation distances. The horizontal axis represents the separation distance between binned, paired data (e.g., all pairs of surface permeability separated by distances between 0 and 3 mm are included in the first bin of Figure 11 discussed later in detail); and the average variance for all paired data in each bin is plotted as a single point along the vertical axis. The resulting plot is known as the experimental semi-variogram and can be best fit by a model semi-variogram that describes the spatial structure of the data characterized by three model parameters – the nugget, sill, and range of spatial auto-correlation. The projected discontinuity near the origin of the plot, known as the *nugget*, represents both the measured parameter error (in our study, the error associated with both the collection and measurement of surface permeability using AutoScan II) as well as the spatial sources of variation at distances smaller than the shortest sampling interval **(**Journel and Huijbregts, 1978). If two surface permeability measurements taken from the same location along the surface of a specimen have no sampling or laboratory error, the values should be the same (i.e., result in a nugget = 0). The *range* (also referred to as the decorrelation distance) is the distance at which the measured variable is no longer spatially correlated. The value of semi-variance associated with the model plateau is defined as the *sill*.

4 RESULTS OF PERMEABILITY CHARACTERIZATION

Surface gas permeability measurements were collected at varying spatial resolutions to demonstrate the versatility and comparability of the AutoScan II and TinyPerm II in characterizing a broad range of natural and engineered porous building materials. Surface permeability data for three representative specimens, Ohio Sandstone, Red Clay Brick, and 3,000 psi Concrete, are presented first to highlight the notable trends. Subsequently, the surface gas permeability data collected at 1 mm grid spacing on 17 internal specimens are presented to facilitate comparisons across a variety of materials.

4.1 AutoScan II Surface Permeability Measurements on Select Materials

An example of measured surface gas permeability on the 70 mm diameter Ohio Sandstone specimen 2 (Figure 3a) at 2 mm grid spacing over a 50 mm diameter circular area using AutoScan II is presented in Figure 3b. The same data are plotted in Figure 3c, where the permeability measurements at given y-coordinates are distributed along the horizontal axis. Figure 3d shows the probability density function (PDF) of the specimen's permeability. The peak of the PDF is the "most observed" value (63.4 mD) and is often used to "globally" characterize the overall permeability. The arithmetic mean, 76.3 mD, geometric mean, 74.3 mD, and the median, 76.5 mD are provided for comparison. The lower permeabilities (i.e., 40s and 50s mD) are located in the mid to lower right portion of the core surface, but most measurements are distributed between 60 and 90 mD. The maximum, minimum, and standard deviation are 140.7 mD, 28.2 mD, and 17.3 mD, respectively. Table 1 presents a summary of these measurements.

The Red Clay Brick specimen 2 (Figure 4a), an example store-bought engineered material, is less homogeneous than the Ohio Sandstone. The permeability values measured at 5 mm interval over the surface area of 170 mm by 65 mm span more than three orders of magnitude, so permeability readings have been $\log_{10}$-transformed. The most observed permeability value is $10^{3.87}$ or 7,414mD, which is closer to the arithmetic mean, 7,102 mD, than the geometric mean, 4,564 mD, and the median, 4,800 mD. The maximum, minimum, and standard deviation are 79,090 mD, 71 mD, and 8,088 mD, respectively (Table 1).

Surface gas permeability was measured along one side of a screeded slab of 3,000 psi Concrete approximately 260 mm × 180 mm × 75 mm (Figure 5a). The permeability was measured at 4 mm grid spacing over a 240 mm by 152 mm area, resulting in 2,331 surface permeability measurements (Figure 5b, where white squares indicate no reading). The surface permeability data, replotted in Figure 5c, generally range from 10 to 80 mD, with a few points outside this range. Figure 5d shows the most observed value of permeability at approximately 41.5 mD, which is close to the arithmetic mean, 42.89 mD, geometric mean, 40.2 mD, and the median, 42.9 mD. The maximum, minimum, and standard deviation are 167 mD, 7.6 mD, and 15.2 mD, respectively (Table 1).

While the surface of the 3,000 psi Concrete specimen of Figure 5 was smoothed and finished with the screeding process, the interior is expected to be more representative of a typical concrete mixture that includes cement paste and fine and coarse aggregates. The permeability measurements made on the screeded surface, in all likelihood, involve only mortar as a result of the screeding process. A comparison between the permeability of a screeded concrete surface (Figure 6a) and the interior surface ~2 mm below the screeded top (Figure 6b) was therefore investigated using a 70 mm core of 3,000 psi Concrete (a different specimen from the slab shown in Figure 5). The surface permeability was measured on the screeded exterior surface, and on the exposed surface after cutting a 2mm slice off of the core using AutoScan II. The $\log_{10}$(mD) permeability fields of each surface (Figures 6c and 6d, respectively) were measured over a 35mm × 35 mm area with 0.5 mm grid spacing.

Both the screeded surface and the interior surface show similar spatial patterns in the surface permeability. These patterns exhibit the expected less permeable "islands" where aggregates are surrounded by thinner, more permeable borders of mortar. While the emerging shapes suggest similar spatial patterns of permeability, the magnitudes differ. Most notable is that the screeded surface permeability measurements are overall approximately one order of magnitude greater than the surface permeability measurements of the interior surface. The presence of aggregates near the measurement surface probably limited gas flow from entry to exit point along the assumed hemispherical flow path, resulting in smaller permeability.

4.2 Comparison of AutoScan II Gas Permeability of Different Porous Building Materials

Using AutoScan II, we characterized 17 interior core specimens using a consistent 35 mm × 35 mm area with 1 mm grid spacing. All cores were extracted from central portions of the specimens, which reduced surface alterations due to screeding or weathering. The specimens discussed in this section are different than those discussed in the previous section (Figures 3-5), even when the specimens share the same parent material. Table 2 summarizes the results of the AutoScan II surface permeability testing along with global statistics (i.e., arithmetic mean (mD), geometric mean (mD), most observed (PDF peak in mD), maximum (mD), minimum (mD), standard deviation (mD)) used to characterize the materials. Photographs of each specimen with its measured 35 mm × 35 mm surface permeability field are presented in Figure 7. The data range over more than five orders of magnitude. Therefore, all surface permeability maps use the same $\log_{10}$(mD) color scale (bottom of Figure 7) for easier visual comparison, where dark blue is less than 1 mD and dark red is greater than 100,000 mD. Grid locations at which a steady-state permeability measurement was not produced are shown in white.

Surface permeabilities of the studied materials ranged from less than 1 mD to over 140,000 mD. Granite is the least permeable with a geometric mean of 0.76 mD, and the Red Colored Brick Paver is the most permeable with a geometric mean of 23,689 mD. Asphalt has the largest number of locations where a steady-state permeability measurement could not be achieved, likely due to the many surficial air pockets.

The global surface permeability characterization was observed to be affected by whether the material is natural or engineered. Most of the natural materials have very low permeabilities, as do the two concretes cured for specified strengths. The four most permeable materials were engineered materials not designed for a specific strength. The 5,000 psi concrete specimen includes a small area of high permeability measurements. This may be indicative of an indentation or imperfection such as a crack along the surface.

4.3 Comparison of AutoScan II and TinyPerm II Measurements

To investigate how well TinyPerm II may characterize a specimen in the field compared to AutoScan II laboratory measurements, each specimen's averaged (geometric mean) permeabilities, measured using TinyPerm II and AutoScan II, are plotted in Figure 8. The geometric mean is less susceptible to outliers or erroneous data. The two geometric means are highly correlated (ρ = 0.97). The 1:1 line is provided for comparison. Overall, the global specimen permeabilities using each of the devices are very similar.

As noted in Section 3.2, TinyPerm II is typically recommended for specimens with a surface permeability greater than 10 mD, yet many of the measurements were below that threshold and required measurement times beyond five minutes. Our results show that overall the specimen characterization appeared to be accurate even below the manufacturer's recommended 10 mD. Hence the limiting factor, when characterizing low permeability materials, is the allotted maximum time required for sampling and not the accuracy of the device itself. It is worth noting that the ranking (either ascending or descending order) of the results with TinyPerm II is similar to that of AutoScan II (Fig. 8), as also indicated by a very high Spearman correlation coefficient which was computed to be 0.97. This suggests that regardless of differences in values, TinyPerm II may be useful for field characterization and selection of sampling points.

4.4 Surface versus Bulk Permeability

The average surface permeability (geometric mean, n=4 specimens) for each material measured with AutoScan II is plotted against the average bulk permeability in Figure 9 with a one-to-one line and a least-squared regression model with an adjusted R^2 of 0.61 (n= 60). The solid, horizontal lines represent the range of the four most observed $\log_{10}$-transformed surface gas permeability values for each material, while the vertical dashed lines indicate the range of the bulk gas permeability measurements for that material. The latter are within one order of magnitude of each other, with the exception of 3,000 psi Concrete, which spans almost two orders of magnitude. Natural materials are plotted with darker symbols while engineered materials are plotted in light gray.

The natural materials (Ohio Sandstone, Arkose Sandstone, Indiana limestone), Red Clay Brick and Portland Cement, are relatively homogeneous and are located close to the one-to-one line in Figure 9, indicating that differences between the surface and bulk gas permeability measurements are relatively small. The remaining materials are fairly heterogeneous (at least for the size of the specimens) engineered materials (Ready Mix Concrete, 3,000 psi Concrete, 5,000 psi Concrete, D04 Concrete, and Red Colored Brick Paver) and contain aggregates. Measurements deviate further from the one-to-one line in Figure 9, suggesting that the bulk permeability of the entire specimen is somewhat different than that of the specimen surface. Given that the concrete specimen surfaces were smoothed and finished via screeding while the interior core is more representative of the heterogeneous mixture, the interior aggregates likely create a longer and more tortuous flow path in bulk permeability measurements, resulting in the smaller observed values of bulk permeability. With the exception of the Arkose Sandstone 2 and Clay Brick, all other materials had greater surface gas permeability measurements than bulk permeability measurements. This bias is likely due to the more tortuous flow path through the entire specimen.

5 EFECTS OF WEATHERING ON PERMEABILITY

In general, surface permeability measured with AutoScan II and/or Tiny Perm II is more similar to bulk permeability for the relatively homogenous materials in this study (natural stones, Red Clay Brick, and Portland Cement) compared to the more heterogeneous engineered materials (i.e., concretes and pavers). The latter is not surprising; and as a result, for applications involving surface contamination or surficial weathering, the use of bulk permeability might not be appropriate, and the surface permeability is probably more suitable.

The surface permeabilities of nine select building materials were tested using AutoScan II before and after weathering simulated using freeze-thaw cycles. The selection of the specific materials was such that there were both natural and engineered materials represented. After weathering, however, specimens from three materials (3,000 psi and 4,000 psi Concretes and Portland Cement) were degraded to the point where they could not be tested. Thus, only specimens from the six fairly intact materials (Ready Mix, 5,000 psi and High Strength Concretes, Red Brick, Indiana Limestone and Arkose Sandstone) were tested and presented here. Figure 10 plots the geometric mean permeability of unweathered specimens on the x-axis and weathered specimens on the y-axis; a 1:1 line is shown for comparison. The natural materials and the ready mix fall on or close to the 1:1 line; however, the latter does so to a slightly lesser degree than the natural materials. All other engineered specimens are substantially farther away from and lie above the 1:1 line, indicating that their surface permeability had increased with weathering. The weathering process produced notable cracks and possibly increased the size of the pores or fractures/openings, facilitating air flow through the specimen. Consequently, the materials have higher surface permeability after weathering, and the use of AutoScan II enables characterization of the weathering effects at high spatial resolution.

The natural materials were considerably less affected by weathering than the engineered materials examined in this study. One possible explanation may be related to the extended period of time that natural materials took to form compared to the relatively rapid curing time allowed for engineered materials. Further studies are necessary to improve our understanding of the underlying mechanism as many factors can have significant influence on the weathering process (e.g., Goudie, 1999; Elert et a;., 2003; Benavente et al., 2004; Scherer, 2004; Flatt et al., 2014). The less homogeneous materials might be more susceptible to weathering damage since tensile stresses are more likely to develop as a result of non-uniform volume expansion/shrinkage. It is important to note that the 5,000 psi Concrete had similar surface permeability to the natural materials before weathering, so the original surface permeability before weathering takes place is probably not a good indicator of resistance to weathering or long-term preservation. However, the increase in permeability with weathering may provide a reliable means to quantify the degree of weathering.

6 GEO-STATISTICAL ANALYSIS OF SURFACE PERMEABILITY

AutoScan II is well suited for acquiring surface permeability data at high resolution and with high precision when evaluating spatial autocorrelation and anisotropy, which is relevant in identifying preferential flow paths inherent in natural materials or modeling flow and transport in building materials. A detailed geo-statistical analysis of the surface gas permeability (mD) measured at 1 mm spacing using AutoScan II along the surface of a slab (306 mm × 114 mm) of Berea Sandstone is shown in Figure 11. Figure 11b shows the corresponding omnidirectional semi-variogram. Variance values associated with paired data have been grouped into 62 equally spaced bins and a typical semi-variogram is produced by plotting the average variance for each bin (small black dots). The semi-variogram shows the measured surface permeability to be spatially auto-correlated at 25 mm. It is possible for the variable in question to become spatially auto-correlated again at larger distances (i.e. where data begin to increase consistently above the sill), resulting in a semi-variogram with multiple decorrelation distances. One important advantage of acquiring data at such high spatial resolution is that we are able to characterize the material's anisotropy. The latter is very important if one wishes to model or predict preferential flow pathways. Figure 11(c) shows the direction of maximum anisotropy to be at 0 degrees (i.e. horizontal direction). It is to be noted that because this was a laboratory specimen, we were able to align the maximum direction with our horizontal x-axis. The directional semivariograms show that the maximum and minimum ranges of spatial autocorrelation to be ~275mm and ~17mm in Figure 11c and Figure 11d, respectively.

Since we did not find this type of material characterization in the literature for the breadth of materials reported here, a similar analysis was performed on all 17 materials; the corresponding values for sill, range, and nugget are listed in Table 2 (see Grover (2014) for further analysis). The omnidirectional range of spatial autocorrelation varied between 5 and 29 mm for the materials tested. However, we were unable to discern any particular trend across materials. The sill on the other hand reveals a significantly larger variance in the engineered materials (0.02 – 1.95 x 10^9, ~11 orders of magnitude) compared to the natural materials (0.003 – 8.5 x 10^3, ~6 orders of magnitude); again, this is an important parameter for modeling flow and transport through the materials' surface as it allows one to quantify the error variance (i.e., uncertainty) associated with the model results.

7 CONCLUSIONS

Surface permeability measurement has been shown to be an effective and reliable non-destructive method for characterizing porous building materials both in the laboratory and in the field. Automated collection and high-resolution measurements render this technique useful for detailed, quantitative characterization of specimen surfaces (e.g. geometric mean, most observed, maximum, and minimum values) and comparisons across specimens.

In general, the measured permeabilities (surface and bulk) compared better to each other for the relatively homogeneous materials of this study (natural stones, Clay Brick and Portland Cement Mortar) than the less homogeneous engineered materials such as concretes. Surface permeability may be easier to measure *in situ*, but it may not be an appropriate surrogate for bulk gas permeability for all materials (e.g. concrete).

Our results indicate that the surface permeability measurements made by TinyPerm II correlate well to those made using AutoScan II. TinyPerm II is compact, portable and easy to use compared to AutoScan II; it is well suited to field use, and it may provide a way to rapidly characterize materials *in situ*. However, it does not allow grid spacing of less than about 3 mm and the measurement point cannot be precisely automated or controlled since it is human operated. In contrast, AutoScan II is well suited when surface permeability data at high resolution and precision are needed. Such high resolution data can enable characterization of the spatial autocorrelation, anisotropy or heterogeneity inherent in building materials.

The high-resolution surface permeability characterization may be necessary for modeling and prediction of preferential flow and transport, as well as quantifying relative changes on the surfaces of porous building materials exposed to effects such as weathering. If the weathering effects related to reduction in material strength, characterizing changes in surface permeability might be used as an indicator of a material’s strength/durability over time, especially in harsh climates. These measurements illustrate the operational effectiveness of the surface permeability measurement techniques, which is particularly relevant to investigations involving surface effects.

8 ACKNOWLEDGMENTS

Support for this work was provided by the Defense Threat Reduction Agency (HDTRA1-08-C-0021), and in part from Vermont EPSCoR with funds from the National Science Foundation Grant EPS-1101317 as well as The University of Vermont’s McNair, URECA!, and the Barrett Foundation undergraduate research programs.

9 REFERENCES

ASTM International. (2002), Annual Book of ASTM Standards: section four, volume 04.08. Soil and Rock (I).

Benavente, D, Garcıa del Cura, M. A., Fort, R. and Ordonez, S. O. (2004). Durability estimation of porous building stones from pore structure and strength. Engineering Geology, 74: 113-127.

Chandler, M. A., Goggin, D. J., and Lake, L. W. (1989) A mechanical field permeameter for making rapid, non-destructive, permeability measurements, J. Sediment. Petrol., 59, 613–615.

Dandekar, A. Y. (2006), Petroleum reservoir rock and fluid properties. CRC Press, 496. ISBN 0849330432.

Davis, J. M., Wilson, J. L., and Phillips, F. M. (1994) A portable air-minipermeameter for rapid in situ field measurements, Ground Water, 32, 258–266.

Dreyer, T., Scheie, A., and Jensen, J. L. (1990) Minipermeameter-based study of permeability trends in channel sand bodies, AAPG Bull., 74, 359–374.

Dullien, F. A. L. (1992), Porous Media Fluid Transport and Pore Structure, 2nd ed. Academic Press, 574. ISBN 0122236505.

Dutton, S. P. and Willis, B. J. (1998) Comparison of outcrop and subsurface sandstone permeability distribution, Lower Createaceous Fall River Formation, South Dakota and Wyoming, J. Sediment. Res., 68, 890–900.

Eijpe, R. and Weber, K. J. (1971) Mini-permeameters for consolidated rock and unconsolidated sand, AAPG Bull., 55, 307–309.

Flatt, R.J., Caruso, F., Sanchez, A. M. A. and Scherer, G. W. (2014). Chemomechanics of salt damage in stone. Nature Communications, 5: 4823 doi: 10.1038/ncomms5823.

Elert, K., Cultrone, G., Navarro, C.R. and Pardo, E. R. (2003). Durability of bricks used in the conservation of historic buildings - influence of composition and microstructure. Journal of Cultural Heritage, 4: 91-99.

Figg J. W. (1972). Determining the water content of concrete panels. *Magazine of Concrete Research*. 24(79): 94-96.

Filomena, C. M., J. Hornung, and H. Stollhofen (2013) Assessing accuracy of gas-driven permeability measurements: a comparative study of diverse Hassler-cell and probe permeameter devices, Solid Earth Discuss., 5, 1163–1190.

Fossen, H., Schultz, R. A., and Torabi, A. (2011) Conditions and implications for compaction band formation in the Navajo Sandstone, Utah, J. Struct. Geol., 33, 1477–1490.

Gladden, L. F., M. H. M. Lim, M. D. Mantle, A.J. Sederman, and E. H. Stitt (2003), MRI visualization of two-phase flow in structured supports and trickle-bed reactors, Catalysis Today 79, doi:10.1016/S0920-5861(03)00006-3.

Goggin, D. J. (1993) Probe permeametry: is it worth the effort?, Mar. Petrol. Geol., 10, 299–308.

Goggin, D.J., R.L. Thrasher, and L. W. Lake (1988), A theoretical and experimental analysis of minipermeameter response including gas slippage and high velocity flow effects, *In Situ*, 12, 79-116.

Goudie, A. S. (1999). A comparison of the relative resistance of Limestones to frost and salt weathering, Permafrost Periglac. Process, 10: 309-316.

Grover, D. K. W. (2014) Surface Gas Permeability of Porous Building Materials: Measurement, Analysis and Applications, M.S. thesis, The University of Vermont.

Hornung, J. and Aigner, T. (2002) Reservoir architecture in a terminal alluvial plain: an outcrop analogue study (Upper Triassic, Southern Germany). Part 1: Sedimentology and petrophysics, J. Petrol. Geol., 2, 3–30.

Huysmansa, M., Peetersa, L., Moermansa, G., and Dassarguesa, A. (2008) Relating small-scale sedimentary structures and permeability in a cross-bedded aquifer, J. Hydrol., 361, 41–51.

Journel, A. G., and Huijbregts, C., 1978, Mining Geostatistics: New York, Academic Press.

Isaaks, E. H. and Srivastava, R. M. (1989), Introduction to applied geostatistics, Oxford University Press, New York, 561 pp.

Iversen, Bo V., P. Moldrup, P. Schjønning, and O. H. Jacobsen (2003) Field Application of a Portable Air Permeameter to Characterize Spatial Variability in Air and Water Permeability, Vadose Zone Journal 2:618–626.

Jang, S. H., M. G. Wientjes, D. Lu, and L. S. A. Jessie (2003), Drug delivery and transport to solid tumors, Pharmaceutical Research, 20 (9), 1337-1350.

Klinkenberg, L. J. (1941), The permeability of porous media to liquids and gases, Drilling and Productions Practices, 200-213.

Lomborg, B. (2000). The Skeptical Environmentalist: Measuring the Real State of the World. Cambridge University Press, 138. ISBN 0521804477.

New England Research (2008), AutoScan Automatic Multi-Sample Measurement Platform; Gas Permeability manual, New England Research, Inc.

New England Research (2014), AutoScan, , New England Research, Inc. available at: http://www.ner.com/site/images/autoscan/NER_AutoScan_2014.pdf (last accessed June 24, 2015):

New England Research, (2015) TinyPerm II Portable Air Permeameter, User's Manual, New England Research Inc. and Vindum Engineering, available at: http://www.vindum.com/wp-content/uploads/TinyPermManual.pdf (last accessed: June 24, 2015).

Rogiers, B., Beerten, K., Smeekens, T., and Mallants, D. (2011) Air permeability measurements on Neogene and Quaternary sediments from the Campine area: using outcrop analogues for determining hydrodynamic aquifer properties, Belgian Nuclear Research Center, Mol, Belgium, External Report SCKCEN-ER-177.

Scherer, G. W. (2004). Stress from crystallization of salt. Cement and Concrete Research, 34: 1613-1624.

Sharp Jr., J. M., Fu, L., Cortez, P., and Wheeler, E. (1994) An electronic minipermeameter for use in the field and laboratory, Ground Water, 32, 41–46.

Steele, B. C. H., and A. Heinzel (2001), Materials for fuel-cell technologies, Nature, 414, 345-352.

Valek, J., J. J. Hughes and P. J. M. Bartos, (2000), Portable probe gas permeability: a non-destructive test for the in-situ characterization of historic masonry, Mat. and Struc., 33, 194-197.

Zaharieva, R., B.B. François, S. Frederic and E. Wirquin (2003), Assessment of the surface permeation properties of recycled aggregate concrete, Cement & Concrete Composites, 25, 223-232.

Table 1. Summary of surface permeability measurements made on Ohio Sandstone, Red Clay Brick, and 3,000 psi concrete specimens (Figures 3, 4, and 5)

Material	Measurement Details	Surface Permeability (mD)						
		Arithmetic Mean	Geometric Mean	Most Observed	Median	Maximum	Minimum	Standard Deviation
Ohio Sandstone (specimen 2)	2 mm grid spacing over 50 mm diameter circular area	76.3	74.3	63.4	76.5	140.7	28.2	17.3
Red Clay Brick (specimen 2)	5 mm grid spacing over 170 mm x 65 mm area	7,102	4,564	7,414	4,800	79,090	71	8,088
3,000 psi Concrete	4 mm grid spacing over 240 mm x 152 mm area	42.9	40.2	41.5	42.9	167	7.6	15.2

Table 2. Summary of surface permeability measurements made on porous building materials (internal specimens with ends discarded) at 1 mm grid spacing using AutoScan II

		Surface Permeability (mD)								
Material Type	**Origin**	**Arithmetic Mean**	**Geometric Mean**	**Most Observed**	**Maximum**	**Minimum**	**Standard Deviation**	**Range (mm)**	**Sill (mD^2)**	**Nugget (mD)**
Arkose Sandstone	Natural	3.21	2.94	2.05	9.23	1.39	1.50	14	2.12	0.19
Ohio Sandstone	Natural	4.74	4.44	6.82	8.63	2.23	1.68	13	2.99	0.970
Portland Brownstone	Natural	3.84	3.80	3.55	6.00	2.59	0.54	9	0.26	0.016
Bluestone	Natural	0.89	0.87	0.74	1.90	0.68	0.21	4	0.43	0.43
Granite	Natural	0.76	0.76	0.75	1.23	0.64	0.06	11	0.0029	0.0012
Buff Indiana Limestone	Natural	177	160	138	575	39.47	82.32	29	8497	73
Gray Indiana Limestone 1	Natural	5.79	5.72	6.20	8.38	2.68	0.85	10	0.79	0.18
Gray Indiana Limestone 2	Natural	3.64	3.57	3.21	10.47	2.25	0.80	9	0.48	0.037
Silver Indiana Limestone	Natural	5.49	5.46	5.53	7.66	2.55	0.56	9	0.26	0.034
Red Clay Brick	Engineered	3.35	3.26	2.76	5.67	1.95	0.79	27	0.92	0.036
3,000 psi Concrete	Engineered	0.98	0.95	1.08	6.08	0.62	0.35	12	0.14	0.0039
5,000 psi Concrete	Engineered	800	1.66	2,344	140,583	0.95	7,964	5	0.020	0.020
Concrete Paver 1	Engineered	8,376	5,974	5,738	31,181	26.43	5,605	10	38,256,867	316,172
Red Colored Brick Paver	Engineered	29,320	23,689	33,228	86,017	413	14,698	11	194,910,243	4,502,877
Tan Colored Brick Paver	Engineered	6,654	2,664	637	38,151	1.20	7,575	9	68,141,303	568,792
Concrete Paver 2	Engineered	9,988	7,758	4,227	36,225	1.17	6,635	19	54,143,304	622,337
Asphalt	Engineered	317	34.71	140	8,325	0.98	585	16	344,270	181,494

FIGURES

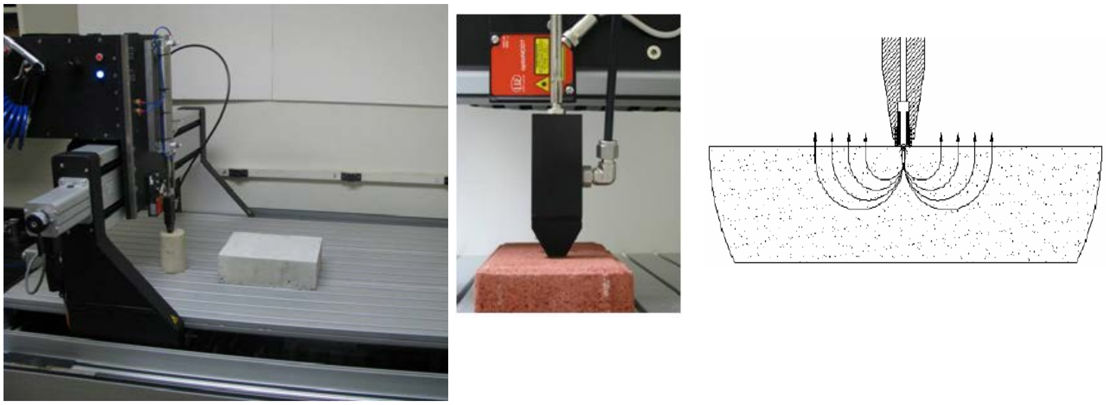

(a) (b) (c)

Figure 1. (a) A laboratory surface permeameter AutoScan II measuring surface gas permeability on multiple specimens, (b) permeability probe on a Red Clay Brick specimen 2, and (c) assumed flow path of injected gas (source: New England Research, 2008).

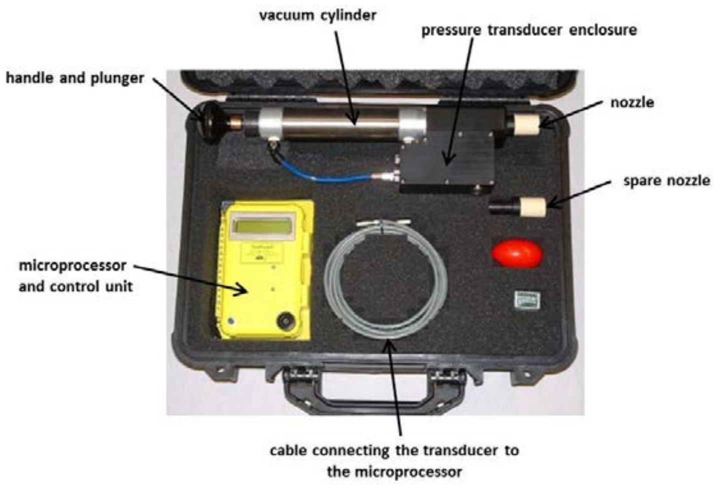

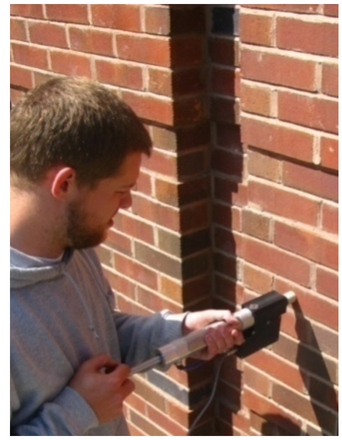

(a) (b)

Figure 2. (a) Components of a portable surface permeameter (TinyPerm II) used in this study (source: New England Research, 2008), and (b) an example of how the device can be used in the field.

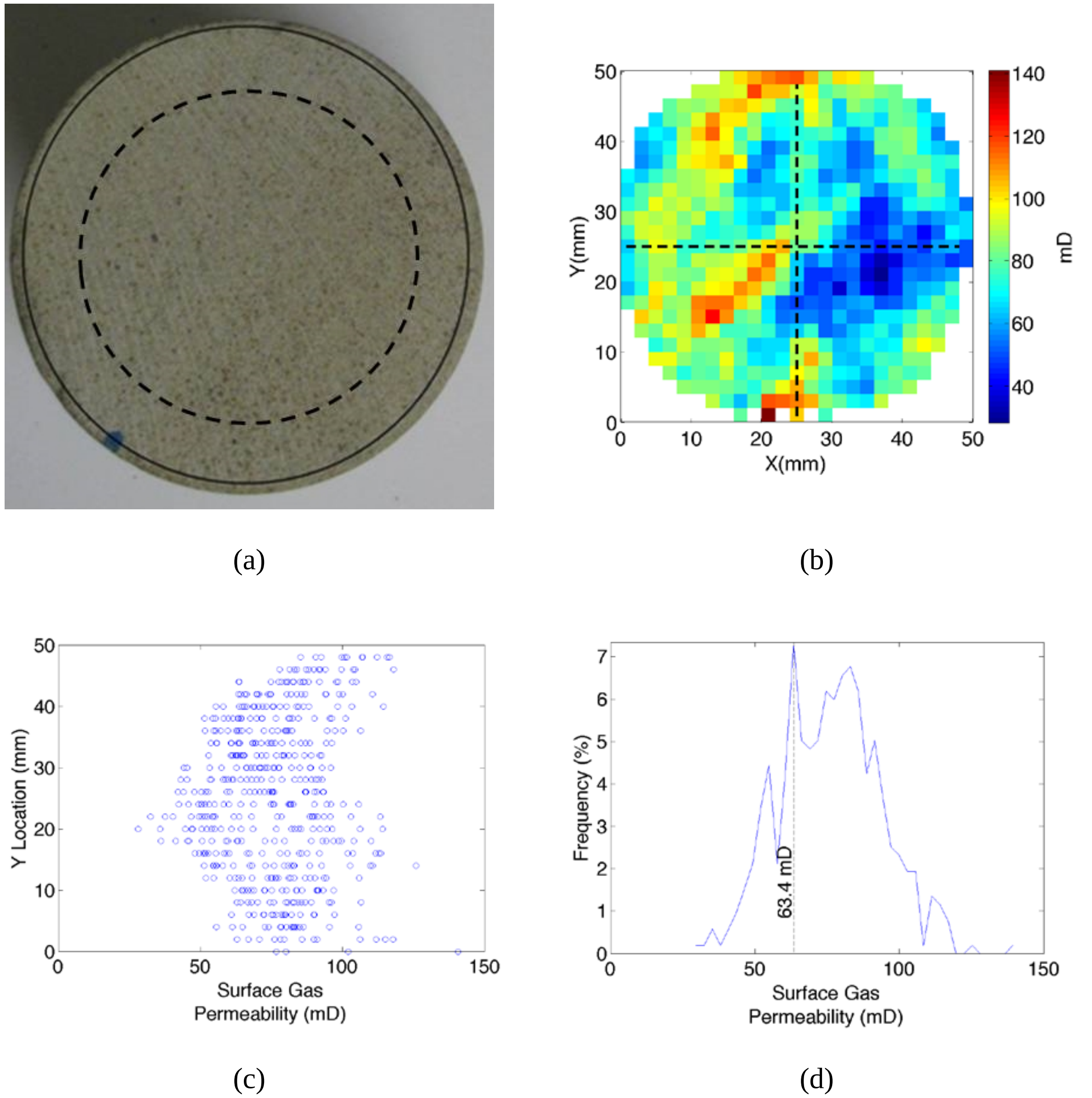

Figure 3. Measured surface gas permeability on a 70 mm diameter Ohio Sandstone specimen 2 at 2 mm grid spacing within the 50 mm diameter circular area shown as a dashed circle, (a) a photograph of the tested surface of the specimen, (b) map of gas permeability, (c) distribution of gas permeability along each y-coordinate, (d) probability density function of gas permeability, most observed value is indicated.

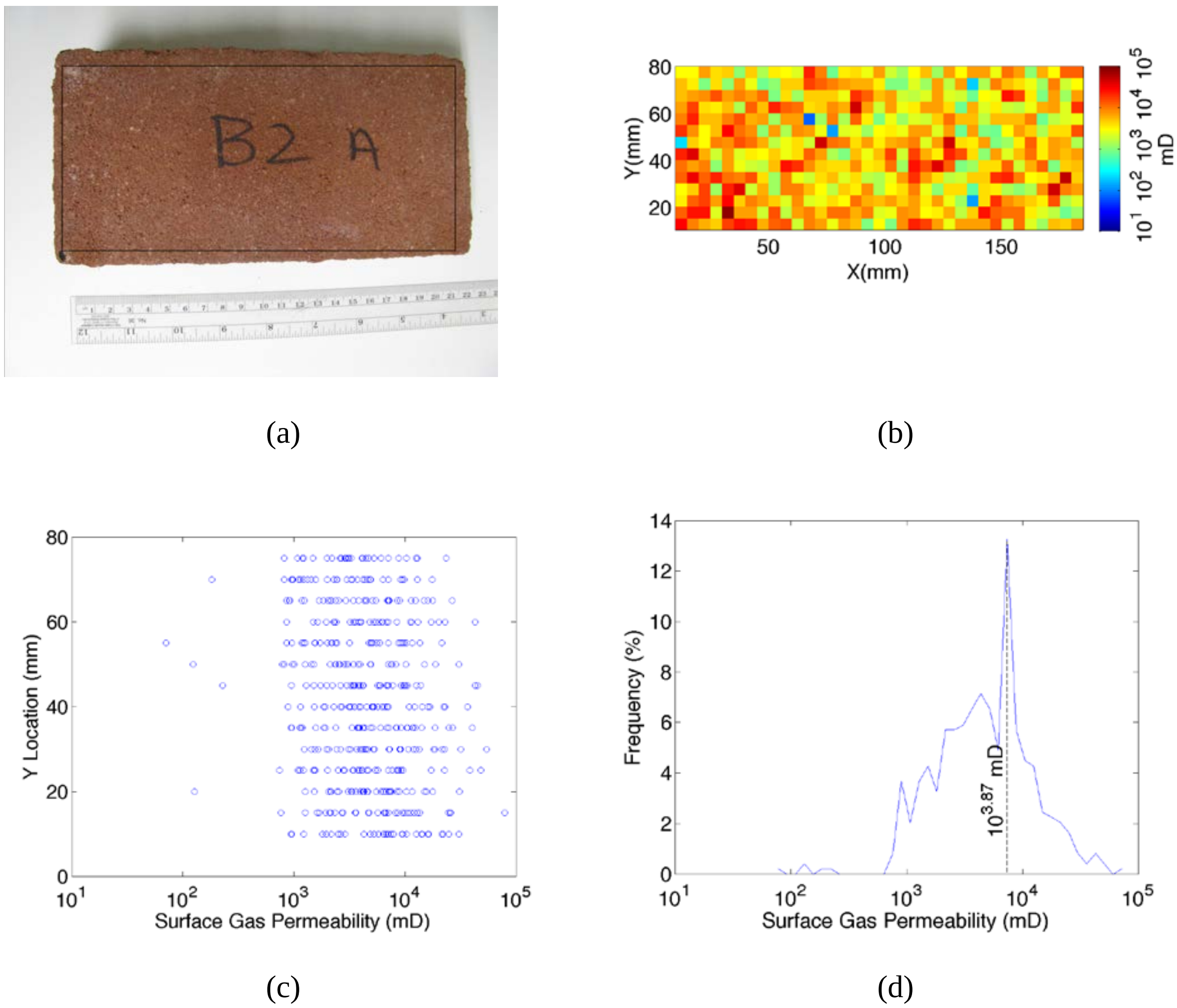

Figure 4. Measured surface gas permeability on a store-bought Red Clay Brick specimen 2 at 5 mm grid spacing over the surface area of 170 mm x 65 mm, (a) a photograph of the tested surface of the specimen, (b) map of surface gas permeability, (c) distribution of surface gas permeability along each y-coordinate, (d) probability density function of gas permeability.

(a)

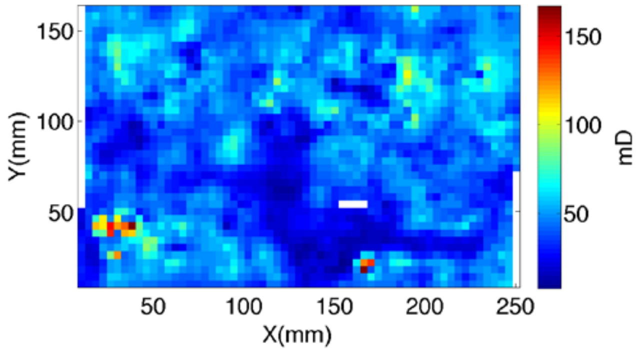

(b)

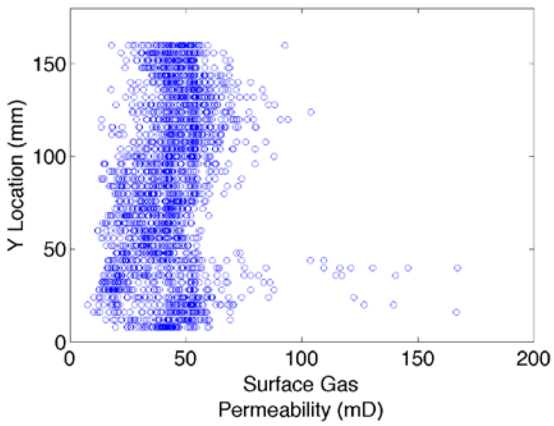

(c)

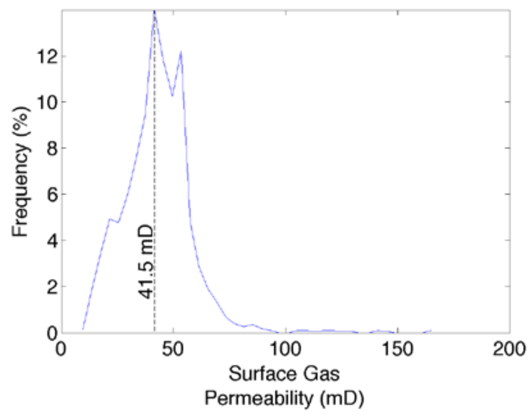

(d)

Figure 5. Measured surface gas permeability on a screeded 3,000 psi Concrete specimen at 4 mm grid spacing over the surface area of 240 mm x 152 mm, (a) a photograph of specimen surface, (b) map of gas permeability field, (c) distribution of gas permeability along each y-coordinate, (d) gas permeability probability density function.

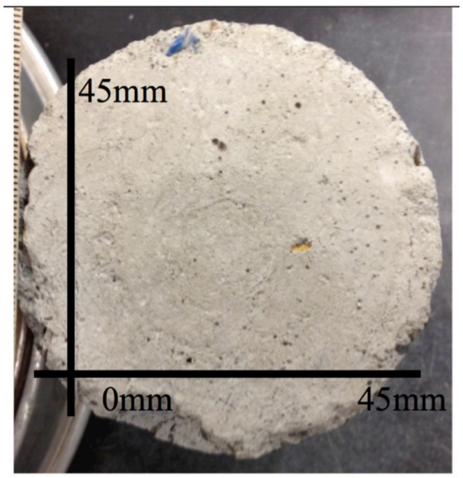

(a)

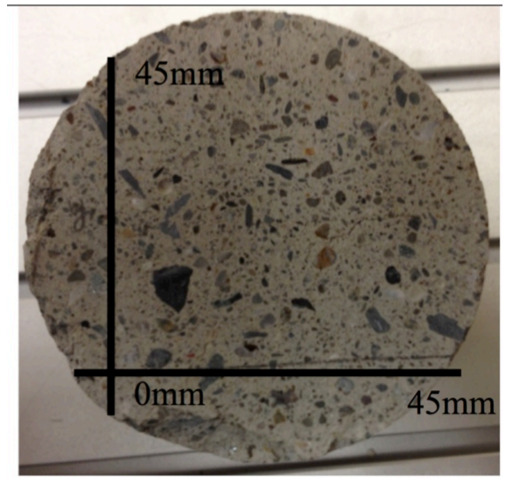

(b)

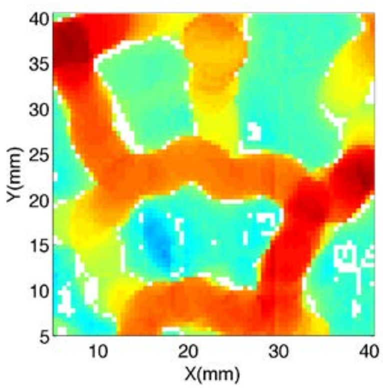

(c)

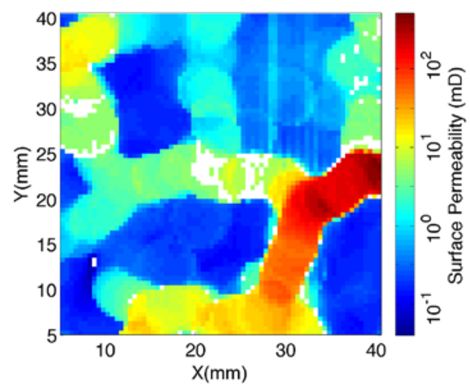

(d)

Figure 6. Core (70 mm diameter) of 3,000 psi Concrete specimen (a) Picture of screeded top, (b) picture of interior about 2 mm below screeded top, (c) surface gas permeability map of the screeded top, (d) surface gas permeability map of on the interior surface. White areas did not return a measurement

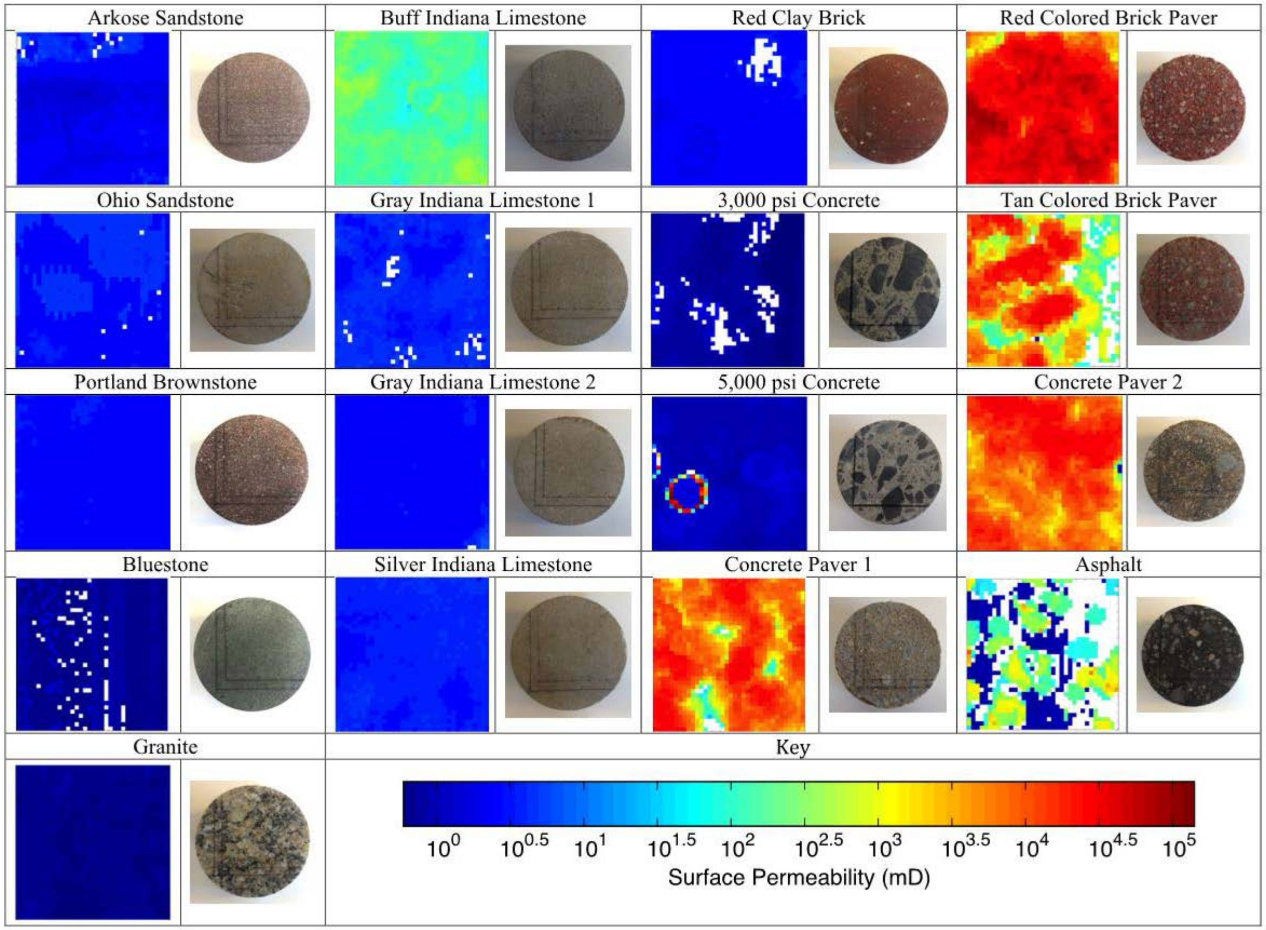

Figure 7. Photographs and surface permeability of the building materials specimens. The natural materials are in the left two columns, and the engineered materials are to the right.

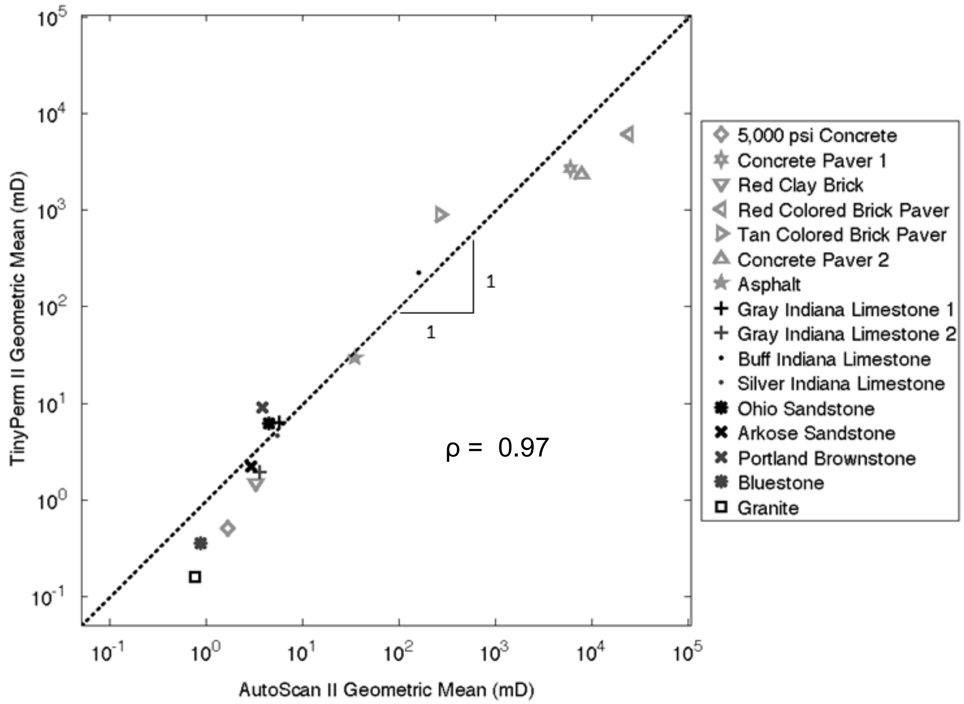

Figure 8. TinyPerm II averages (geometric mean) versus AutoScan II averages (geometric mean). Natural materials are shown as black or dark gray while engineered materials are show as light gray. Both data sets were $\log_{10}$ transformed, and the correlation coefficient $\rho = 0.94$.

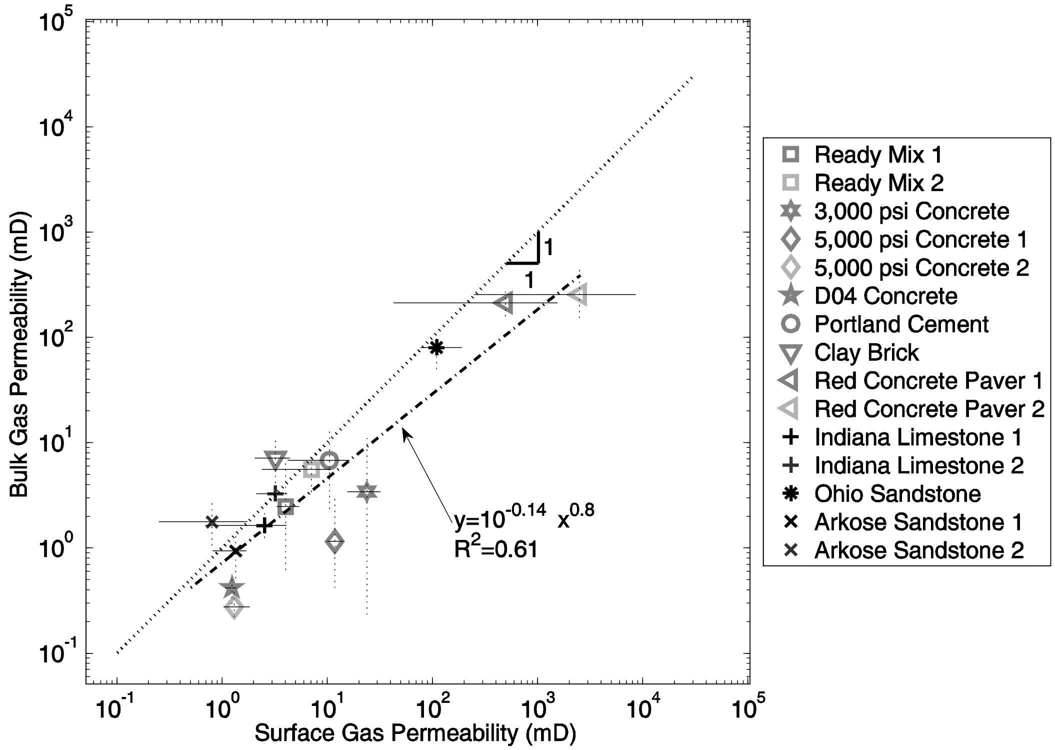

Figure 9. Bulk gas permeability plotted against geometric mean of surface gas permeability obtained using AutoScan II. The natural materials (e.g. Indiana, Ohio and Arkose Sandstone) are depicted with black symbols, while the engineered materials (all Concretes, Brick, and Pavers) are depicted in lighter gray.

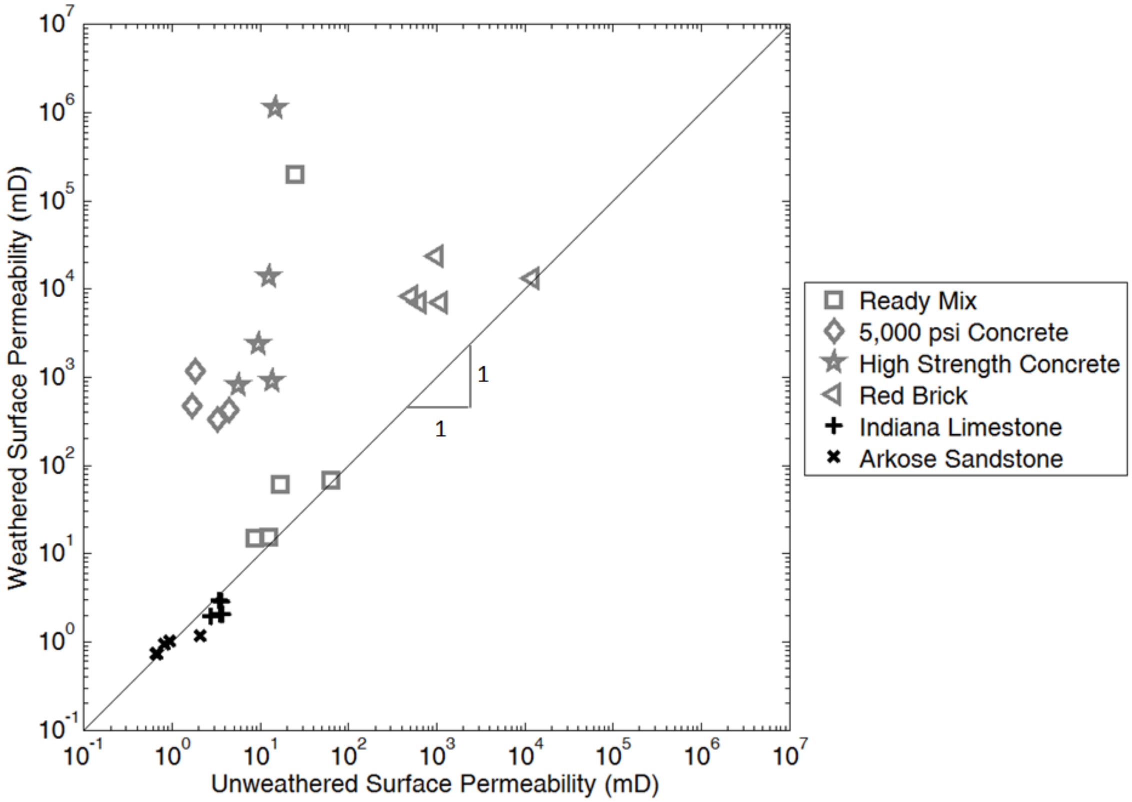

Figure 10. Comparison of specimen geometric mean permeabilities obtained using AutoScan II under unweathered and weathered conditions. The natural materials (Indiana Limestone and Arkose Sandstone are depicted with black symbols, while the engineered materials (all Concretes and Brick) are depicted in lighter gray.

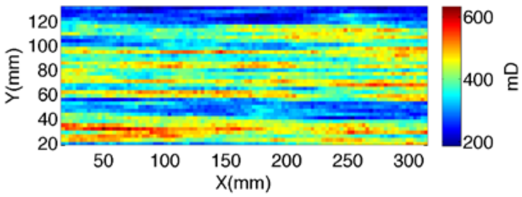

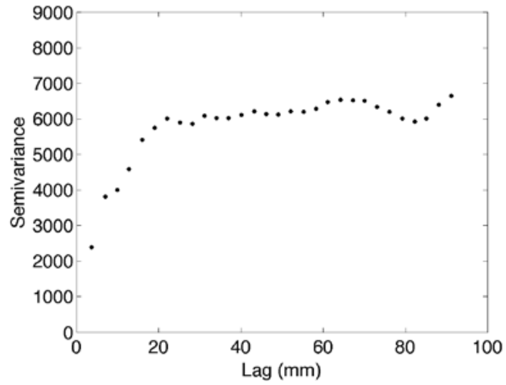

(a) (b)

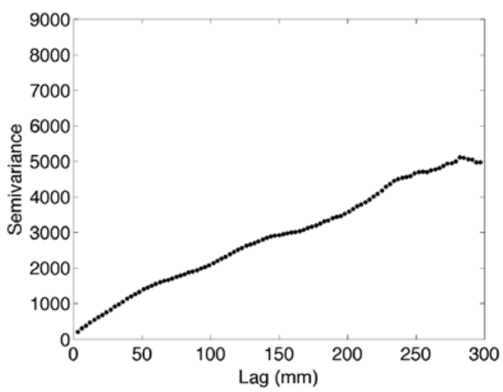

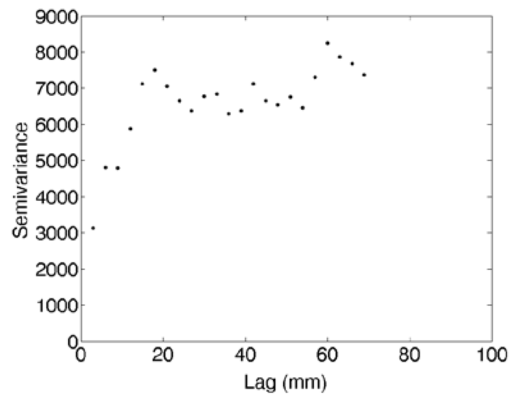

(c) (d)

Figure 11. (a) The surface gas permeability (mD) measured along the surface of a Berea Sandstone slab (1 mm spacing); the corresponding (b) omnidirectional semi-variogram analysis (model: spherical, range: 25 mm, sill: 6,063, nugget: 1,600); (c) horizontal semivariogram at 0^o (model: linear, range: 275 mm, sill: NA, nugget: 200); and (d) vertical semivariogram at 90^o (model: spherical, range: 17 mm, sill: 7,200, nugget: 2000).

Graphical Abstract

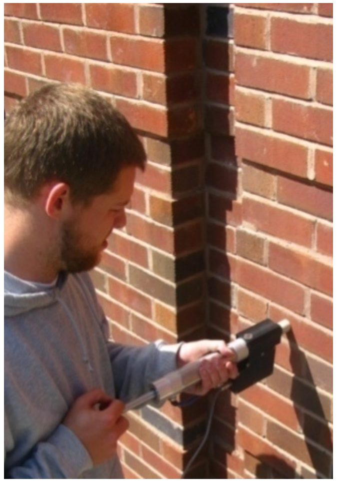

Hand-held field surface gas permeameter (TinyPerm II)

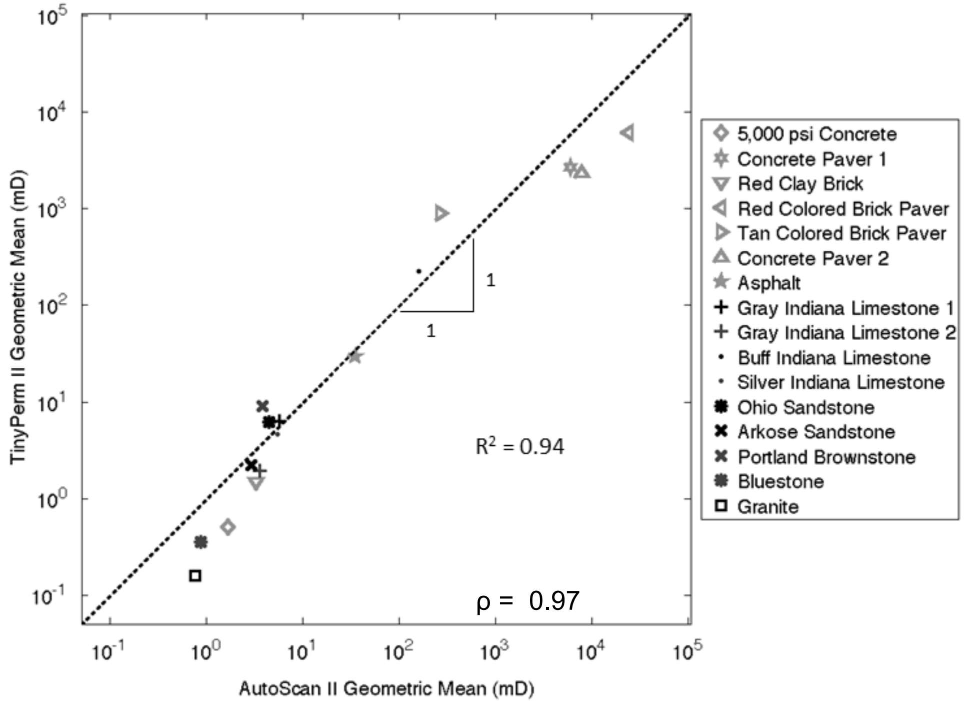

Applications:

1. Correlation with bulk gas permeability
2. Degree of degradation from weathering (e.g. freeze-thaw)
3. Quantification of spatial autocorrelation, heterogeneity and anisotropy

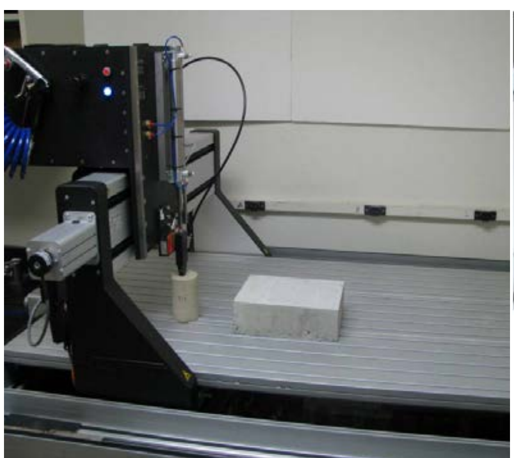

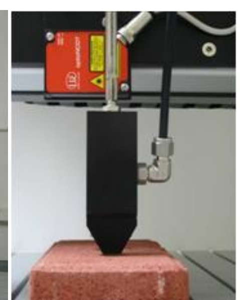

Laboratory surface gas permeameter (AutoScan II)

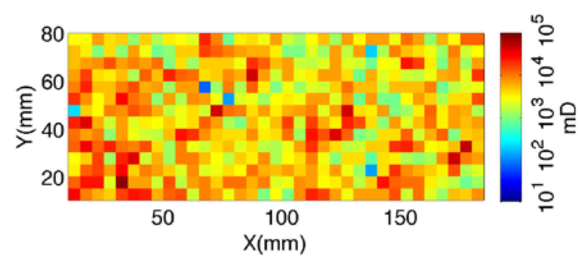

Surface permeability map of the brick specimen (shown to the left)